Direct imaging of exoEarths embedded in clumpy debris disks

D. Defrère*[a], C. Stark[b], K. Cahoy[c], and I. Beerer[c]

[a] Max-Planck-Institut für Radioastronomie, Auf dem Hügel 69, 53121 Bonn, Germany
[b] Carnegie Institution of Washington, 5241 Broad Branch Rd. NW, Washington, DC 20015, USA
[c] Massachusetts Institute of Technology, 37-367, 77 Massachusetts Ave., Cambridge, MA 02139, USA

ABSTRACT

The inner solar system, where the terrestrial planets formed and evolve, is populated by small grains of dust produced by collisions of asteroids and outgassing comets. At visible and infrared wavelengths, this dust cloud is in fact the most luminous component in the solar system after the Sun itself and the Earth may appear similar to a clump of zodiacal dust to an external observer. Hence, the presence of large amounts of dust in the habitable zone around nearby main-sequence stars is considered as a major hurdle toward the direct imaging of exoEarths with future dedicated space-based telescopes. In that context, we address in this paper the detectability of exoEarths embedded in structured debris disks with future space-based visible coronagraphs and mid-infrared interferometers. Using a collisional grooming algorithm, we produce models of dust clouds that simultaneously and self-consistently handle dust grain dynamics, including resonant interactions with planets, and grain-grain collisions. Considering various viewing geometries, we also derive limiting dust densities that can be tolerated around nearby main-sequence stars in order to ensure the characterization of exoEarths with future direct imaging missions.

Keywords: ExoEarth imaging, exozodiacal dust, space telescope, coronagraphy, interferometry, matched filter.

1. INTRODUCTION

The inner solar system, where the terrestrial planets formed and evolve, is populated by small (1-100 μm) grains of dust produced by collisions of asteroids and outgassing comets. This zodiacal dust cloud (also referred to as a debris disk) fills the ecliptic plane within the asteroid belt and can be clearly seen from Earth as a diffuse glow in the night sky. At visible and infrared wavelengths, it is in fact the most luminous component in the solar system after the Sun itself and the Earth may appear similar to a clump of zodiacal dust to an external observer.[1] Hence, the possible presence of dust in the habitable zone around nearby main-sequence stars is considered as a major hurdle toward the direct imaging of Earth-like extrasolar planets (exoEarths) with future dedicated space-based telescopes. On the one hand, exozodiacal dust is a source of background noise that significantly contributes to photon noise and, hence, to the integration time required for detecting a planet. Also, structures in exozodiacal clouds are potential sources of confusion that might bias the planet detection and produce false positives. On the other hand, these structures might nonetheless represent signposts of unseen perturbing planets and may motivate close inspection of the planetary systems where they are detected.

Dust structures in debris disks have been predicted by various theoretical studies[2–4] and observed later around several stars.[5–7] The origin of some of these clumpy structures may be attributed to the gravitational influence of planets on the small dust grains. After their release from parent bodies via collisions or outgassing, dust grains experience different paths in the stellar system, depending on their effective size. Whereas the smallest particles are ejected from the planetary systems by radiation pressure in a dynamical time, larger particles slowly spiral inward due to Poynting-Robertson drag. While spiraling toward their host star, dust particles may become temporarily trapped in exterior mean motion resonance with planets, extending their lifetimes. This trapping

* E-mail: ddefrere@mpifr-bonn.mpg.de, Telephone: +49-(0)228-525-353

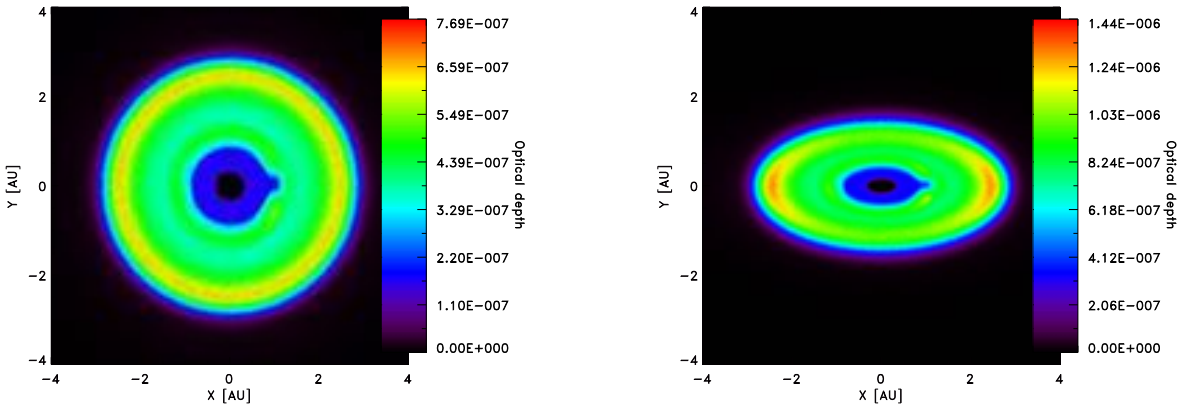

Figure 1. Geometric optical depth for two representative 1-zodi disk models, showing the resonant dust structures created by an Earth-like planet orbiting on a circular orbit at 1 AU from the star with an inclination of 0° (left figure) and 60° (right figure). The planet is located on the x-axis (90 degrees clockwise from vertical).

locally enhances the particle density, creating structures, originally described for the solar zodiacal cloud as circumstellar rings, bands, and clumps leading and trailing the Earth in its orbit.[1]

Unfortunately, very little is currently known about the presence of dust in the habitable zone region of nearby planetary systems. So far, debris disks have mostly been observed on relatively large spatial scales, corresponding to material located tens to hundreds of AU from their host star. Whether exozodiacal dust is actually present in observable quantities in all exoplanetary systems has been an important question for several years. Mid-infrared surveys (e.g., IRAS, ISO, *Spitzer*) addressed this issue and reported the detection of warm dust (at $\sim$10 μm) around a handful of candidates with an occurrence rate lower than 1% for nearby main-sequence stars and a detection threshold of $\sim$1000 times the zodiacal dust emission.[8] A more sensitive survey with infrared interferometry found only 3 detections in a survey of 25 targets and derived an upper limit for the mean exozodiacal dust density of 150 zodis (3-σ upper limit, corresponding to 99% confidence under the additional assumption that the measurement errors are Gaussian).[9]

In this paper, we investigate the impact of exozodiacal dust structures on the exoEarth imaging with future space-based coronagraphs and mid-infrared interferometers (the impact of exozodiacal dust as background noise as been extensively discussed elsewhere[10,11]). Using a collisional grooming algorithm, we produced models of dust clouds that simultaneously and self-consistently handle dust grain dynamics, including resonant interactions with planets, and grain-grain collisions.[12] These modeled images are then used as input of our instrument simulators and help us to address the detectability of an exoEarth orbiting at 1 AU around a Sun-like star located at 10 pc.

2. THE EXOZODIACAL DUST DISK MODEL

Exozodiacal dust cloud models with resonant ring structures were produced using a collisional grooming algorithm.[12] Briefly, this algorithm simultaneously solves the equations of motion governing small dust grains, including the interactions with a planet on a circular orbit around the star, and the number flux equation including destruction of dust grains via grain-grain collisions. The algorithm uses a collisionless debris disk "seed model" as input and iteratively solves the number flux equation until the three-dimensional dust distribution matches that of a steady-state collisional disk with a given dust production rate. A more detailed explanation of the collisional grooming algorithm can be found in Stark et al. (2009).[13]

For the present study, we focus on disk models of a Sun-Earth system located at 10 pc and surrounded by a dust disk of various densities (from 1 to 100 zodis where we define a 1-zodi model as having a maximum face-on geometric optical depth of 10^{-7}, similar to the optical depth of the zodiacal cloud). Each of these models integrated the orbits of 12,500 dust grains launched from a belt of parent bodies exterior to the orbit of the

planet. A hybrid symplectic integrator with an integration step size equal to one hundredth of the period of the planet was used and the parent body orbits were distributed uniformly in semi-major axis between 2.5 a_p and 3.0 a_p, uniformly in eccentricity between 0 and 0.1, and uniformly in inclination between 0° and 10°. All other parent body orbital parameters were distributed uniformly between 0 and 2π. The resulting model is shown in Fig. 1 for two different representative cases. Note that our models are artificially truncated at a distance of 0.3 AU for the sake of clarity but the missing dust is symmetric and would not affect the analysis presented in this paper.

3. IMAGING EXOEARTHS WITH OPTICAL TELESCOPES

3.1 Instrumental concept

We consider in this section an optical telescope equipped with a Phase Induced Amplitude Apodization Coronagraph (PIAAC[14]) but the results discussed here should be similar for other optical wavelength missions using either external occulters or internal coronagraphs. In short, the PIAA coronagraph provides lossless amplitude apodization of the pupil by geometric redistribution of light instead of selective absorption.[15] The geometrical remapping of the telescope pupil amplifies phase slopes, therefore enabling observations at smaller angular separations than with a conventional amplitude apodization. A focal plane mask occults starlight in the first focal after two aspheric optics (mirrors or lenses) are used for the beam remapping. Then, an inverse pair of beam remapping optics are used to restore the original pupil and recover the field of view.

The coronagraph simulation was performed with a modified version of the one described by Guyon et al. (2006)[14] using the parameters listed in Table 1. The present PIAAC simulation considers a 4-meter diameter telescope aperture observing a Sun-like star located at 10 pc with an Earth-sized planet in a circular orbit at 1 AU. Including stellar leakage and zodiacal dust emission, the simulator produced the images shown in Fig. 2 (no photon noise) and in Fig. 3 (with photon noise) for various disk densities.

3.2 The need for exozodiacal background subtraction

Despite the apparent gap in the exozodiacal dust distribution near the planet position (see Fig. 1), a significant background emission from the exozodiacal cloud is mixing with that of the planet. This is because the hole is not completely devoid of dust and because part of the surrounding emission is likely to fall within the telescope PSF (depending on its size, target distance, etc..). Hence, as a first step, we computed the amount of exozodiacal flux that falls within the PSF at the planet position and compared it to the planet flux. The corresponding ratio is shown in Fig. 2 with respect to the disk density for various disk inclinations. This figure clearly shows that the exozodiacal dust emission is generally dominant from a typical ratio of a few tenths for a few zodis to 0.1% for the edge-on system of 100 zodis. Whereas this exozodiacal flux directly contributes to increased background noise and, hence, longer exposure times, it also represents a source of confusion and a possible bias on the planet detection. It is therefore important to accurately remove the exozodiacal background emission in the image obtained by the coronagraph. The technique usually proposed to get around this issue is to fit an exozodiacal disk model to parts of the image and then subtract the model from the image. This technique has the advantage

Table 1. Coronagraphic simulation parameters used in this study (see more details in Guyon et al. 2006[14]).

Parameter	Value	Comment
Coronagraph type	PIAAC	Phase-induced amplitude apodizing coronagraph[14]
Telescope diameter	4 m	
Imaging wavelength	550 nm	Bandwidth of 110 nm
Wavefront quality	Perfect	No time-variable wavefront errors
Detector	Perfect	No readout noise or dark current included
Star	1.3×10^{8} ph m^{-2} s^{-1}	Sun-like at 10 pc
Planet	9.5×10^{-3} ph m^{-2} s^{-1}	ExoEarth at 1 AU, albedo of 0.2
Exozodiacal dust	1 to 100 zodis	Collisional disk model with resonant structures[12]
Zodiacal background	23.28 to 22.24 m$_V$/arcsec^2	Function of ecliptic latitude
Integration time	10000 s	About 7 hours

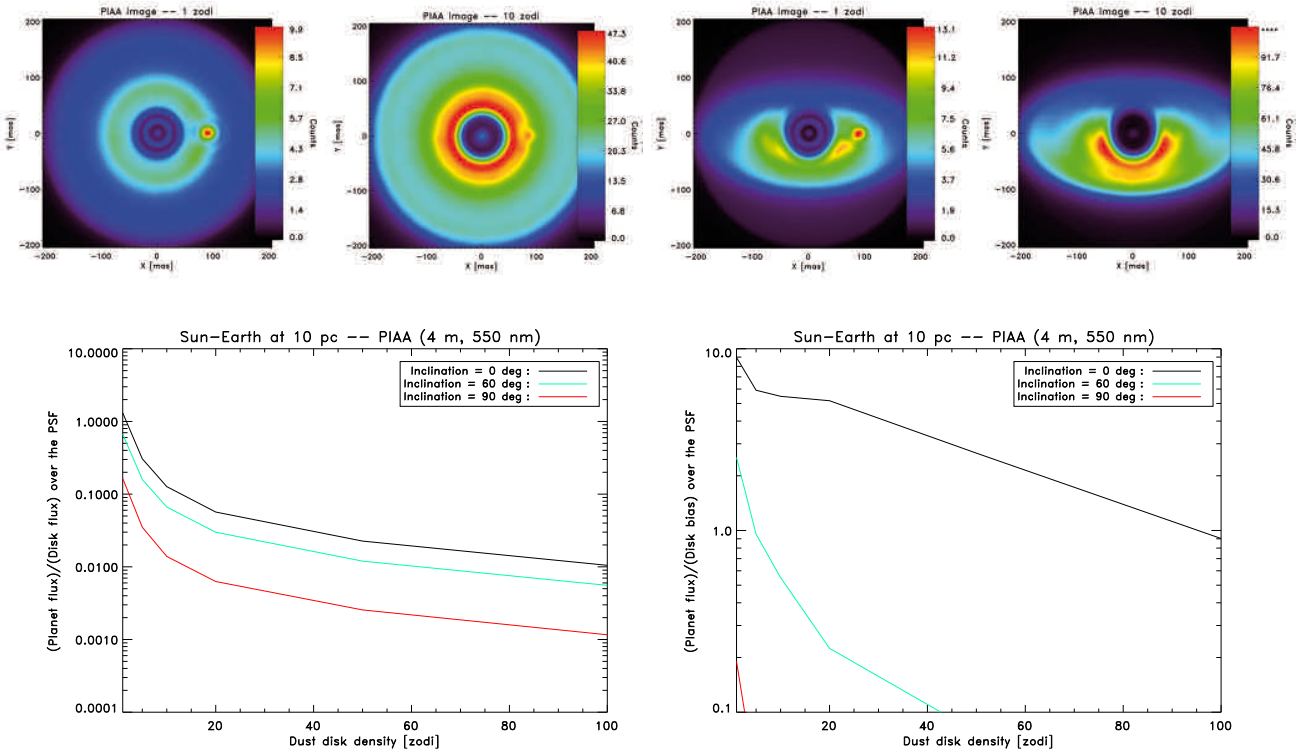

Figure 2. *Top,* Simulated images produced by the PIAA coronagraph (no Poisson noise) for two dust disk densities (1 and 10 zodis, left figures) and two disk inclinations (0° and 60°, right figures). *Bottom*, Amount of exozodiacal background within the PSF at the planet position compared to the planet flux for various disk inclinations (left figure). The right figure shows the corresponding bias after removing an azimuthally-averaged exozodiacal disk model.

to remove smoothly varying exozodi emission fairly easily but can lead to significant biases if the model used for the fit is not appropriate and does not account properly for the flux at the planet position. Representative exozodiacal disk models like that presented in the previous section will be therefore of crucial importance to analyze and model the images obtained by future space-based coronagraphs.

It would not be appropriate to use our input model as a background estimator since this would lead to a perfect background subtraction and would not represent the uncertainties that we will face in reality with actual images of planetary systems. Instead, we used an azimuthally-averaged version of our model as an estimator of the exozodiacal background. Although quite restrictive, this approach provides a good estimate of typical biases inherent to the model fitting of the exozodiacal background. The ratio of the planet flux to the bias at the planet position (averaged over the PSF) is shown in Fig. 2 (bottom right) for various disk densities. A more detailed analysis is currently under progress and will be presented in an upcoming paper (Stark et al., in prep). In the following, we focus on the face-on case since the azimuthally-averaged image is not a very good estimator for inclined disks.

3.3 Planet signal extraction

In order to assess the detectability of the exoEarth in the images produced by the PIAA simulator, we performed a matched-filtering algorithm (or PSF fitting) which has been shown to be close to the optimal linear detection strategy.[16] In short, matched filtering consists in subtracting the background model from the images produced by the coronagraph and then cross-correlating the results with the Point Spread Function (PSF) of the telescope. To derive the signal-to-noise ratio (SNR) at each position, the matched-filtered images are then divided by the photon noise map at each position (see result in the SNR maps displayed in Fig. 3 computed for an integration

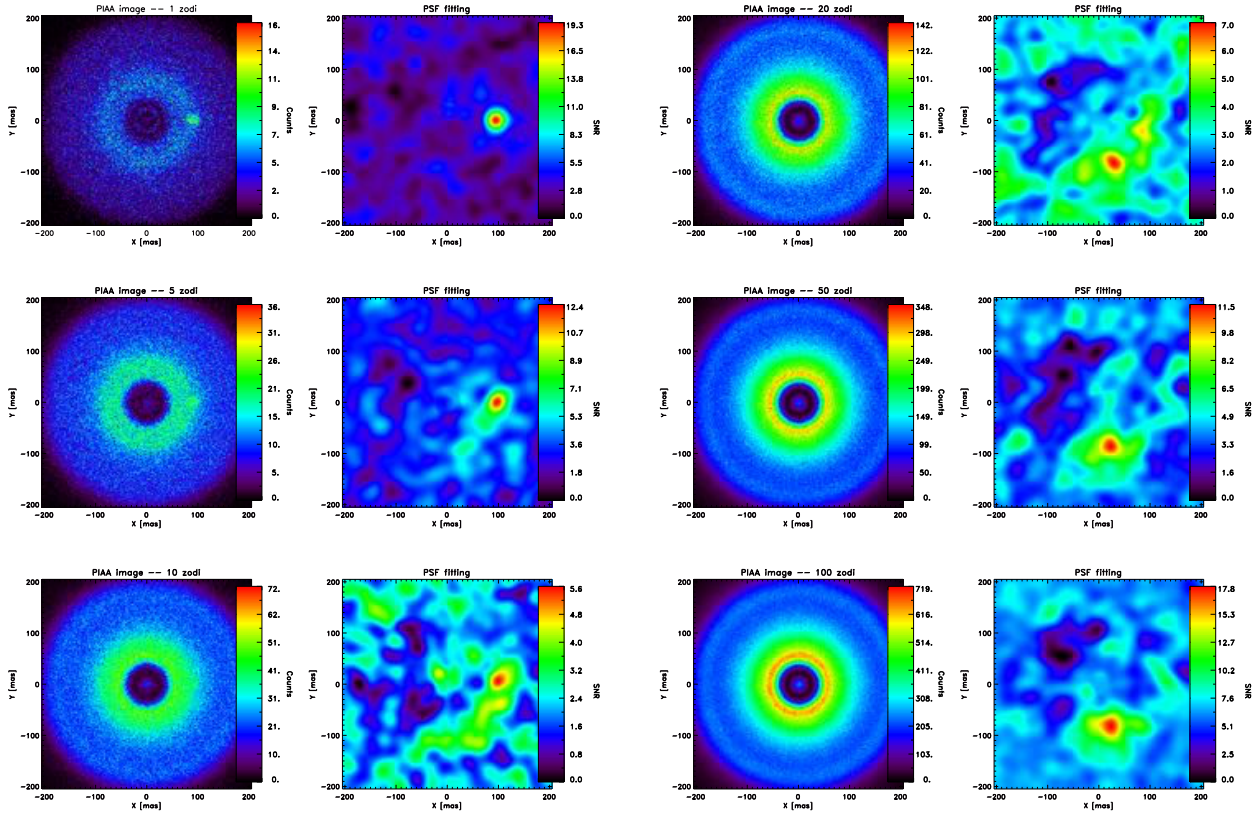

Figure 3. Images produced by the PIAA coronagraph and corresponding result of the PSF fitting for a Sun-Earth system located at 10 pc and surrounded by an exozodiacal cloud of various densities (left column: 1, 5, and 10 zodis; right column: 20, 50, and 100 zodis).

time of 10000 s, approximately 7 hours). For the lowest exozodiacal dust densities ($\lesssim$20 zodis), Fig. 3 shows that there is a clear detection at the planet position (SNR>5) although our background model, equivalent to the azimuthally-averaged image, over-estimates the exozodiacal emission at the planet position and a part of the planet flux is removed by the background subtraction. This dust density of 20 zodis must therefore be considered as a very conservative upper limit.

In addition, at approximately 10 zodis, a second clear detection appears in the SNR map at a few degrees behind the planet on its orbit. This detection corresponds to planet-trailing grains which are present in our input model and observed in the Zodiacal cloud. These planet-trailing grains dominate the detection map at dust densities higher than 15 zodis and represent a significant source of confusion. At this stage, a spectroscopic analysis might offer the best chance of revealing the nature of this detection. While spectroscopic analysis is not in the scope of this paper, it is an area of active research. It is also interesting to note that the planet-trailing clump remains detectable up to at least 100 zodis and acts as a signpost indicating the presence of a nearby planet. If such a clump is detected, one can make a strong case for spending a longer time integration time on this target to reveal the planet.

4. IMAGING EXOEARTHS WITH MID-INFRARED INTERFEROMETERS

The detection and characterization of exoEarths in the mid-infrared present several advantages, including a better contrast with the star than in the visible (10^7 for a Sun-like star compared to 10^{10} in the visible) and the presence of spectral bands of water, carbon dioxide, and ozone. However, resolving the habitable zone around nearby stars in the mid-infrared requires a very large telescope with a diameter of at least 20 m. Space-based

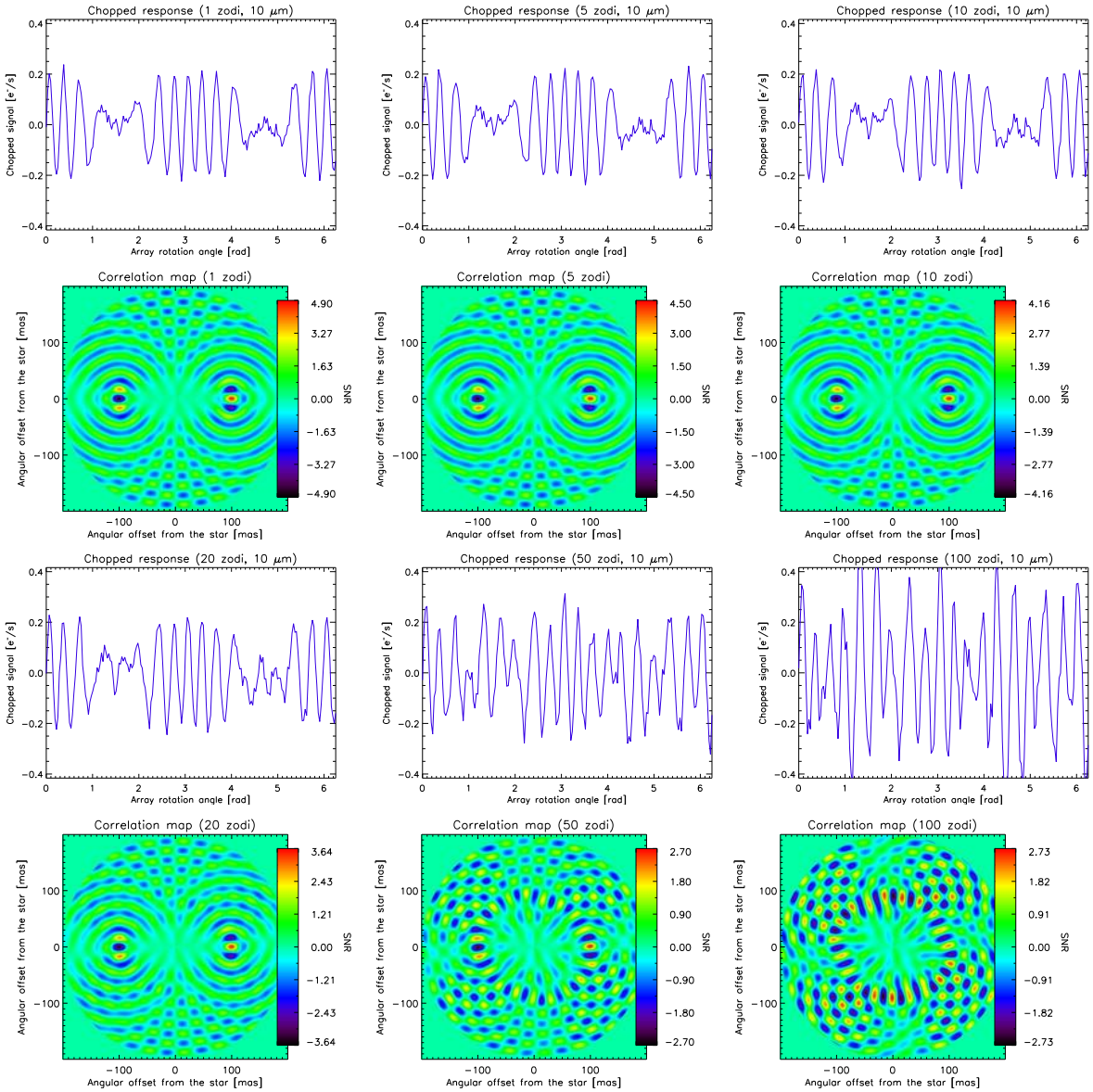

Figure 4. Simulated chopped photon rate as a function of the array rotation angle for various exozodiacal dust densities and corresponding correlation maps computed for an Emma X-array nulling interferometer.

interferometry is therefore considered as the most promising technique to achieve this goal. During the past decade, substantial effort was made to define a design that provides excellent scientific performance at minimum cost and technical risk. This has resulted in a convergence and general consensus on a single mission architecture consisting of a non-coplanar X-array, called Emma, using four collector spacecraft and a single beam combiner spacecraft.[17] Such a design enables the implementation of phase chopping, a technique which suppresses from the final output all sources having point-symmetric brightness distributions. Hence, most of the exozodiacal dust emission is removed by phase chopping and there is no need for background subtraction by model fitting. Nonetheless, asymmetric structures (such as the planet-trailing clump described above) are not suppressed and thereby contribute as possible biases and/or false positives.

In this study, we consider the mission architecture described by Table 2 and performed the simulations with the DARWINsim software which was previously used to assess the impact of exozodiacal dust on the detection

Table 2. Interferometric simulation parameters used in this study (see more details in Defrère et al.(2010)[18]).

Parameter	Value	Comment
Interferometer type	Emma X-array	4 telescopes with phase chopping[17]
Telescope diameter	4 m	
Baseline	11×66 m	Optimized configuration
Imaging wavelength	10 μm	Bandwidth of 0.5 μm
Instrumental stability	Perfect	No optical-path difference nor intensity mismatchs
Detector	Perfect	No readout noise or dark current included
Star	1.7×10^6 ph m^{-2} s^{-1}	Sun-like at 10 pc
Planet	0.17 ph m^{-2} s^{-1}	ExoEarth at 1 AU
Exozodiacal dust	1 to 100 zodis	Collisional disk model with resonant structures[?]
Zodiacal background	7.1×10^{12} ph m^{-2} s^{-1} sr^{-1}	Kelsall model[1]
Integration time	80 h	About 3.3 days

of exoEarths.[18] Introducing our new model images into DarwinSIM, we computed the total chopped photon rate as a function of the array rotation angle for a face-on system of various exozodiacal dust densities. The results are represented in Fig. 4 with the corresponding correlation maps below (obtained by cross-correlation of the chopped signal with the expected signal of a point source at each position). This figure shows that the planet can be detected up to 20 zodis with a SNR of at least 3. Unlike the coronagraph, there is no significant detection (SNR>3) of false positives beyond 20 zodis and at least up to 100 zodis.

5. CONCLUSION

Using a collisional disk model,[12] we addressed in this paper the impact of resonant dust structures in exozodiacal disks on the detection of exoEarths with future space-based visible coronagraphs and mid-IR interferometers. Considering a Sun-Earth system located at 10 pc, we showed that the flux of the exozodiacal dust falling within the PSF at the planet position is generally dominant and must therefore be accurately removed. Using a simple axi-symmetric model for the exozodiacal background subtraction however, produces a significant bias at the planet position, even for disks with a density as low as 1 zodi. This suggests that a detailed modeling of the exozodiacal dust disk, using models like those presented in this work, will be mandatory in order to ensure the accurate detection of planets. We also performed matched filtering on our simulated images (coronagraph) or chopped signals (interferometer). In both cases, the detection of the planet becomes challenging beyond a density of approximately 20 zodis in a reasonable integration time. In the case of the coronagraph, there is in addition a clear false positive produced by grains trailing the planet on its orbit. This false positive is the most easily detected feature beyond 20 zodis and might represent the first detected signpost of a nearby unseen planet. A more detailed analysis considering the effect of target distance, planet longitude, and disk inclination is currently in progress and will be discussed in an upcoming paper (Stark et al. in prep).

ACKNOWLEDGMENTS

DD would like to thank J.-C. Augereau and O. Absil for useful discussions.

REFERENCES

[1] Kelsall, T., Weiland, J. L., Franz, B. A., Reach, W. T., Arendt, R. G., Dwek, E., Freudenreich, H. T., Hauser, M. G., Moseley, S. H., Odegard, N. P., Silverberg, R. F., and Wright, E. L., "The COBE Diffuse Infrared Background Experiment Search for the Cosmic Infrared Background. II. Model of the Interplanetary Dust Cloud," *ApJ* **508**, 44–73 (Nov. 1998).

[2] Roques, F., Scholl, H., Sicardy, B., and Smith, B. A., "Is there a planet around beta Pictoris? Perturbations of a planet on a circumstellar dust disk. 1: The numerical model," *Icarus* **108**, 37–58 (Mar. 1994).

[3] Liou, J.-C. and Zook, H. A., "Signatures of the Giant Planets Imprinted on the Edgeworth-Kuiper Belt Dust Disk," *AJ* **118**, 580–590 (July 1999).

[4] Ozernoy, L. M., Gorkavyi, N. N., Mather, J. C., and Taidakova, T. A., "Signatures of Exosolar Planets in Dust Debris Disks," *ApJ* **537**, L147–L151 (July 2000).

[5] Greaves, J. S., Holland, W. S., Wyatt, M. C., Dent, W. R. F., Robson, E. I., Coulson, I. M., Jenness, T., Moriarty-Schieven, G. H., Davis, G. R., Butner, H. M., Gear, W. K., Dominik, C., and Walker, H. J., "Structure in the ϵ Eridani Debris Disk," *ApJ* **619**, L187–L190 (Feb. 2005).

[6] Krist, J. E., Ardila, D. R., Golimowski, D. A., Clampin, M., Ford, H. C., Illingworth, G. D., Hartig, G. F., Bartko, F., Benítez, N., Blakeslee, J. P., Bouwens, R. J., Bradley, L. D., Broadhurst, T. J., Brown, R. A., Burrows, C. J., Cheng, E. S., Cross, N. J. G., Demarco, R., Feldman, P. D., Franx, M., Goto, T., Gronwall, C., Holden, B., Homeier, N., Infante, L., Kimble, R. A., Lesser, M. P., Martel, A. R., Mei, S., Menanteau, F., Meurer, G. R., Miley, G. K., Motta, V., Postman, M., Rosati, P., Sirianni, M., Sparks, W. B., Tran, H. D., Tsvetanov, Z. I., White, R. L., and Zheng, W., "Hubble Space Telescope Advanced Camera for Surveys Coronagraphic Imaging of the AU Microscopii Debris Disk," *AJ* **129**, 1008–1017 (Feb. 2005).

[7] Schneider, G., Weinberger, A. J., Becklin, E. E., Debes, J. H., and Smith, B. A., "STIS Imaging of the HR 4796A Circumstellar Debris Ring," *AJ* **137**, 53–61 (Jan. 2009).

[8] Lawler, S. M., Beichman, C. A., Bryden, G., Ciardi, D. R., Tanner, A. M., Su, K. Y. L., Stapelfeldt, K. R., Lisse, C. M., and Harker, D. E., "Explorations Beyond the Snow Line: Spitzer/IRS Spectra of Debris Disks Around Solar-type Stars," *ApJ* **705**, 89–111 (Nov. 2009).

[9] Millan-Gabet, R., Serabyn, E., Mennesson, B., Traub, W. A., Barry, R. K., Danchi, W. C., Kuchner, M., Stark, C. C., Ragland, S., Hrynevych, M., Woillez, J., Stapelfeldt, K., Bryden, G., Colavita, M. M., and Booth, A. J., "Exozodiacal Dust Levels for Nearby Main-sequence Stars: A Survey with the Keck Interferometer Nuller," *ApJ* **734**, 67–+ (June 2011).

[10] Absil, O., Defrère, D., Roberge, A., Augereau, J.-C., Coudé Du Foresto, V., Hanot, C., Stark, C., and Surdej, J., "Direct imaging of Earth-like planets: why we care about exozodis," in [*Society of Photo-Optical Instrumentation Engineers (SPIE) Conference Series*], *Society of Photo-Optical Instrumentation Engineers (SPIE) Conference Series* **7734** (July 2010).

[11] Roberge, A., Chen, C. H., Millan-Gabet, R., Weinberger, A. J., Hinz, P. M., Stapelfeldt, K. R., Absil, O., Kuchner, M. J., Bryden, G., and the NASA ExoPAG SAG #1 Team, "The Exozodiacal Dust Problem for Direct Observations of ExoEarths," *eprint arXiv:1204.0025* (Mar. 2012).

[12] Stark, C. C., "The Transit Light Curve of an Exozodiacal Dust Cloud," *AJ* **142**, 123 (Oct. 2011).

[13] Stark, C. C. and Kuchner, M. J., "A New Algorithm for Self-consistent Three-dimensional Modeling of Collisions in Dusty Debris Disks," *ApJ* **707**, 543–553 (Dec. 2009).

[14] Guyon, O., Pluzhnik, E. A., Kuchner, M. J., Collins, B., and Ridgway, S. T., "Theoretical Limits on Extrasolar Terrestrial Planet Detection with Coronagraphs," *ApJS* **167**, 81–99 (Nov. 2006).

[15] Guyon, O., "Phase-induced amplitude apodization of telescope pupils for extrasolar terrestrial planet imaging," *A&A* **404**, 379–387 (June 2003).

[16] Kasdin, N. J. and Braems, I., "Linear and Bayesian Planet Detection Algorithms for the Terrestrial Planet Finder," *ApJ* **646**, 1260–1274 (Aug. 2006).

[17] Cockell, C. S., Léger, A., Fridlund, M., Herbst, T. M., Kaltenegger, L., Absil, O., Beichman, C., Benz, W., Blanc, M., Brack, A., Chelli, A., Colangeli, L., Cottin, H., Coudé du Foresto, F., Danchi, W. C., Defrère, D., den Herder, J.-W., Eiroa, C., Greaves, J., Henning, T., Johnston, K. J., Jones, H., Labadie, L., Lammer, H., Launhardt, R., Lawson, P., Lay, O. P., LeDuigou, J.-M., Liseau, R., Malbet, F., Martin, S. R., Mawet, D., Mourard, D., Moutou, C., Mugnier, L. M., Ollivier, M., Paresce, F., Quirrenbach, A., Rabbia, Y. D., Raven, J. A., Rottgering, H. J. A., Rouan, D., Santos, N. C., Selsis, F., Serabyn, E., Shibai, H., Tamura, M., Thiébaut, E., Westall, F., and White, G. J., "Darwin-A Mission to Detect and Search for Life on Extrasolar Planets," *Astrobiology* **9**, 1–22 (Feb. 2009).

[18] Defrère, D., Absil, O., den Hartog, R., Hanot, C., and Stark, C., "Nulling interferometry: impact of exozodiacal clouds on the performance of future life-finding space missions," *A&A* **509**, A9+ (Jan. 2010).